2014 International Conference on Unmanned Aircraft Systems (ICUAS)
May 27-30, 2014. Orlando, FL, USA

Configuration Assessment and Preliminary Control Law Design for a Novel Diamond-Shaped UAV

Stanislav Braun, Markus Geiser, Matthias Heller, and Florian Holzapfel

Abstract - **The development of a novel aircraft configuration is typically accompanied by high technical risks. In order to ensure the success of such a development, a risk reduction phase must be considered in the design cycle.**

The paper at hand gives insight into the activities related to flight dynamics and control that have been performed during the risk reduction phase of a novel diamond-shaped UAV, the so-called SAGITTA Demonstrator.

In particular, the main design drivers for the configuration's Flight Control System are provided and details on the inherent lateral dynamics and worst case stabilization capability are presented. Furthermore, a preliminary controller structure that is suitable to meet the requirements and an appropriate gain design method are proposed. The resulting preliminary closed-loop system is analyzed in frequency domain (e.g. by means of Nichols charts) and time domain (i.e. gust response). By the activities, summarized as Controllability Study, main requirements are validated and significant development risk reduction is achieved.

Index Terms - **Constrained Eigenstructure Assignment, Controllability, Flight Control System, Flight Dynamics Assessment, Remotely Piloted Aircraft, SAGITTA Demonstrator, Stabilization Capability, UAV**

I. Introduction

THE development of a novel aircraft configuration is typically embedded into a well-structured project life cycle. This life cycle can be divided into seven phases. The first five phases are related to development of the system. These phases are:

- Pre-Phase A: Concept Studies
- Phase A: Concept & Technology Development
- Phase B: Preliminary Design and Technology Completion
- Phase C: Final Design and Fabrication
- Phase D: System Assembly, Integration and Test Launch

Date of current version April 30, 2014. This work was supported by the Technische Universität München – Institute for Advanced Study, funded by the German Excellence Initiative.

All authors are with the Institute of Flight System Dynamics, Technische Universität München, Boltzmannstrasse 15, D-85748 Garching, Germany.
Markus Geiser and Matthias Heller additionally are with the Institute for Advanced Study, Technische Universität München, Lichtenbergstrasse 2a, D-85748 Garching, Germany.
{Stanislav.Braun, Markus.Geiser, Matthias.Heller, Florian.Holzapfel}@tum.de

The remaining two post-production phases are:

- Phase E: Operations and Sustainment
- Phase F: Closeout

Every phase is characterized by a phase-specific purpose, a typical output and multiple reviews, which have the function of quality gates and build the basis for transition to the next phase marked by a so-called Key Decision Point. [1]

In the following, we will focus on the Phases B and C. Our particular interest is in tasks performed during these phases within the scope of design of a Flight Control System (FCS). In this context the main task of Phase B is to develop a realizable concept of the Flight Control System for the novel aircraft configuration under consideration. This encloses, but is not limited to:

- Detailed Requirements Analysis
- Elaboration of Detailed Concept of Operations
- Elaboration of Flight Control System's Architecture
- Specification of Subsystems
- Selection of Equipment

In order to be able to evaluate the suitability and feasibility of the proposed system design, the Flight Control System designer has to validate the requirements and perform a first verification of compliance of the chosen architecture with FCS requirements. For a novel aircraft configuration this means, among other things, to prove the ability to control the aircraft using the control power and sensor feedbacks available in the specified FCS architecture. For this purpose a Controllability Study is conducted, which leads to a better understanding of the achievable flight dynamics of the aircraft and which states the basis for the confirmation of the proposed FCS design. These results enable the FCS designer to successfully pass the quality gate called Preliminary Design Review (PDR) and to proceed to Phase C of the project life cycle.

Whereas Phase B is concerned with elaboration and feasibility of design variants, Phase C is about reduction of the remaining design space to a single design, its implementation and successful defence in the Critical Design Review (CDR).

The aim of this paper is to present details of the development activities, analyses and results that were worked out by the development team of the Flight Control System of the novel diamond-shaped unmanned aircraft, the

so-called SAGITTA Demonstrator in the Phases B and C of the project life cycle. In particular, the Controllability Study, as well as a suitable approach to controller structure definition with aid of Constrained Eigenstructure Assignment (CEA) are presented. The focus will be limited to the aircraft's lateral motion.

II. Preliminaries

A. Aircraft Configuration

The basic aircraft setup under study is a diamond-shaped flying wing configuration with an approximate wingspan of 3 meters and a MTOW of 150 kg. The aircraft is equipped with two integrated jet engines, each providing 300 N of thrust and a retractable tripod landing gear. The basic setup is shown in Fig. 1. In the following, this setup is called "Setup Wing". The wingtips are equipped with novel split flaps, having their hinge line in parallel to the leading edge. Besides the split flaps two independent conventional flaps are installed on each side of the aircraft.

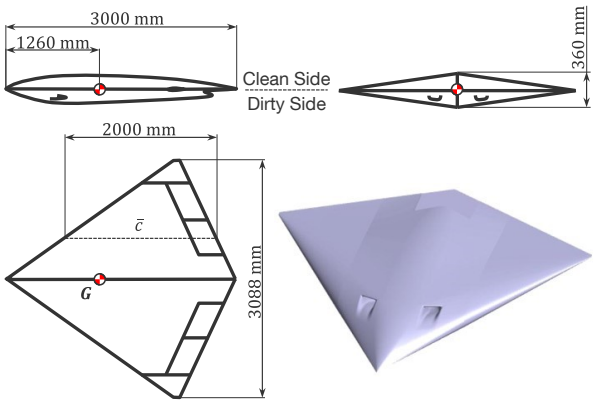

Fig. 1. Basic aircraft setup.

The basic aircraft setup can be changed to the "Setup Wing VT", which implies the attachment of a vertical tail (without additional control surfaces) on the clean side of the aircraft for improvement of lateral stability. A third setup consists of the basic setup, the attachable vertical tail on the clean side, and a gimbaled camera pod on the dirty side of the aircraft. This setup is referred as "Setup Wing VT GBL". All setups must be considered in two configurations: "Landing Gear Retracted" and "Landing Gear Deployed".

B. Design Drivers for the FCS and the Control Laws

For the elaboration of the Flight Control System architecture and the development of control laws, the main design drivers are the following requirements:

- The aircraft shall be flyable in both orientations (with the clean side pointing up- or downwards).
- A skilled RC pilot shall be able to control and land the aircraft without additional visual aids.
- Take-off and landing with a cross-wind of 5.2 m/s must be tolerated by the FCS.
- The max. crab angle at touchdown shall be $\leq 4.5°$

Due to weight and cost limitations, it was decided to implement a simplex Flight Control System architecture. However, to minimize the risk of a loss of the aircraft, the Flight Control System was separated into the main FCS having implemented complex functions up to automatic trajectory following and management of peripherals, and a second system called Basic Flight Control system (BFCS) which shall allow to segregate the Flight Management System in case of malfunction and to ensure continuation of safe flight. Therefore the BFCS shall provide the minimum functionality to safely fly and land the aircraft. To increase the robustness to sensor failures only a minimum number of feedbacks shall be used.

Based on these considerations a basic set of flight state measurements sufficient to stabilize the aircraft and to allow a skilled RC pilot to control and land the aircraft was identified. It was decided, to use the measurements from an Attitude & Heading Reference System (AHRS), since it provides rotation rates for improvement of the damping of the eigenmodes, as well as measurements of lateral and longitudinal accelerations that can be fed back for modification of the eigenmodes' frequency. Furthermore, the AHRS system is considered to be simple and therefore providing a higher degree of reliability, compared to an Inertial Navigation System (INS).

C. Motivation and Goals of the Study

The transition from Phase B to Phase C represents a crossroads in the project development cycle. It is the termination of coexistence of multiple solutions. The designer is asked to select the best suitable approach from a variety of solutions. He must ensure that the selected solution will address the stated requirements and lead to successful implementation in terms of compliance with requirements, available time and cost.

For most aircraft systems that are related to flight dynamics (e.g. Flight Control System or Actuation System) a deeper understanding of the system's open- and closed-loop behavior is required to select an appropriate solution. This is even more important in case of development of a novel aircraft configuration like the SAGITTA Demonstrator, where many unknowns lead to a higher development risk.

In order to validate the design drivers stated in B and to provide a solid base for the validation of the preliminary system design, it was decided to conduct a study with focus on the controllability and flyability of the UAV. A challenge of the study is the stabilization of the aircraft (Setup Wing shows an inherent unstable Dutch Roll Motion for large velocities) using AHRS measurements. Furthermore manual flight and landing conducted by a so-called External Pilot (EP) standing near the runway and piloting the aircraft without additional visual aids shall be evaluated.

In particular, the following points are addressed during the studies for all three setups:

- Confirmation of aircraft's aerodynamic design (in particular, suitability of the novel split flap design for lateral control and stabilization).
- Confirmation of actuator design for aircraft's control surfaces.
- Possibility to stabilize the aircraft using measurements of body's accelerations, rotation rates and its attitude (Euler angles). This requirement

results in a fixed-gain controller that is suitable for the entire flight envelope.

- Elaboration of expected system's closed-loop stability properties.
- Identification of the best suitable command variables for radio-piloting of a poorly visible aircraft (attitude of diamond-shaped UAV poorly identifiable due to the lack of vertical tail and clearly distinguishable wings). Analysis of command variables tracking and aircraft's reaction to gusts.
- Evaluation of closed-loop flight performance by candidate EPs.
- Feasibility of a soft landing (vertical speed limited to 2.5 m/s by landing gear design) by the EP.
- Assess suitability of the Basic Flight Control Computer hardware regarding processing power and resulting latencies.
- Uncover overlooked problems.

D. *Approach*

The study is separated into two parts. Part 1 deals with prototyping of control laws and flight dynamics analysis of the resulting closed-loop systems. In our context, prototyping means derivation of an engineering controller and omitting for the moment the optimization regarding robustness or performance. This part is referred to as the Controllability Study. The second part is called Manual Landing Study and concentrates on virtual flight in Hardware-in-the-Loop Simulation (HILS) tests and their results. The Manual Landing Study will be topic of future papers. In the following, we will focus on the Controllability Study only. Although the study was conducted for all three setups, in order not to exceed this paper, we will provide a deeper insight into the most critical Setup Wing and omit details on other setups.

III. Initial Configuration Assessment

In order to get in touch with the plant dynamics and thus lay the foundations for the later controller design, an initial configuration assessment is conducted.

Linear state space models are a valuable source of insight into the plant dynamics and were hence first of all derived from the nonlinear 6 degrees of freedom simulation model by means of trimming and linearization. We will omit a description of trimming and linearization, however section III.A addresses the applied control allocation.

With the linear state space models at hand, the aircraft's inherent dynamics are examined next. Since the longitudinal and lateral motion of the SAGITTA Demonstrator are sufficiently decoupled, the assessment was conducted with separate state space models for the longitudinal and lateral motion. We will focus on the more critical lateral motion within this paper.

Using novel split flaps, it is of special importance to get an early impression of the yaw controls' capability to stabilize the aircraft. Typically, a respective assessment is conducted by means of (nonlinear) simulation with the final control laws. In contrast to that, we will elaborate on a conservative approach not in need of a controller design in section C.

A. *Control Allocation*

For trimming and linearization three equivalent control surface deflection commands were mapped to the deflection commands for the 8 independent control surfaces with a first control allocation layer as follows:

$$\begin{aligned}
\delta_{old,cmd} &= +\left(\zeta_{equiv,cmd} + |\zeta_{equiv,cmd}|\right)/2 \\
\delta_{olc,cmd} &= -\left(\zeta_{equiv,cmd} + |\zeta_{equiv,cmd}|\right)/2 \\
\delta_{ml,cmd} &= -\xi_{equiv,cmd} \\
\delta_{il,cmd} &= +\eta_{equiv,cmd} \\
\delta_{ir,cmd} &= +\eta_{equiv,cmd} \\
\delta_{mr,cmd} &= +\xi_{equiv,cmd} \\
\delta_{orc,cmd} &= +\left(\zeta_{equiv,cmd} - |\zeta_{equiv,cmd}|\right)/2 \\
\delta_{ord,cmd} &= -\left(\zeta_{equiv,cmd} - |\zeta_{equiv,cmd}|\right)/2
\end{aligned} \tag{1}$$

Thereby $\delta_{il,cmd}$ and $\delta_{mr,cmd}$ represent the deflection commands for the inboard flap of the left hand side respectively the midboard flap of the right hand side. In case of the outboard flaps the trailing c or d indicates that the flap is on the clean respectively dirty side of the SAGITTA Demonstrator.

For simplicity, the control allocation is considered to be part of the plant together with the 2nd order actuator dynamics which are modelled identical for all equivalent control surfaces ($\zeta = 0.7, \omega_0 = 31.4\, rad/s$).

By choosing the clean and dirty side of the outboard flaps to deflect symmetrically, a significant rolling moment is introduced at higher angles of attack by these dedicated yaw effectors. This disadvantage is accepted to allow for inverted flight even with a fixed-gain controller, without the need of reconfiguration.

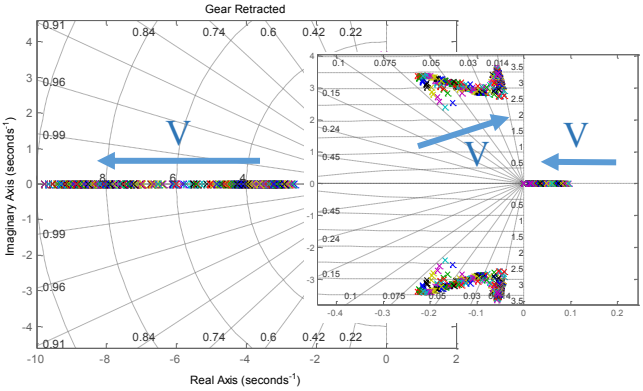

Fig. 2. Inherent lateral dynamics of Setup Wing with retracted landing gear.

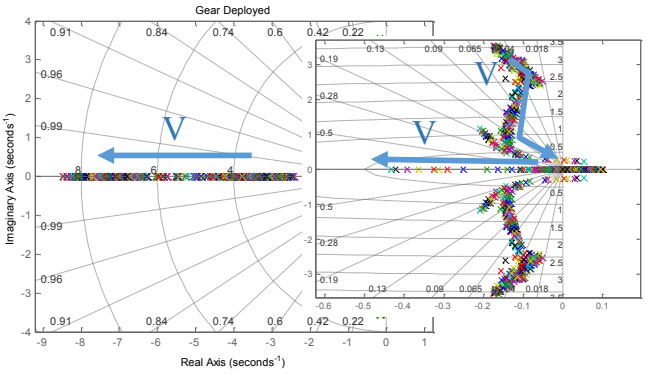

Fig. 3. Inherent lateral dynamics of Setup Wing with deployed landing gear.

B. Eigenmodes of the Plant

Being one of the most basic frequency domain analyses and yet very useful in developing a good understanding for an aircraft's dynamics and their changes over the flight envelope, Fig. 2 and Fig. 3 provide depictions of the poles, i.e. eigenvalues, of the lateral motion of the uncontrolled Setup Wing with retracted respectively deployed landing gear in the complex plane for airspeeds between 30 and 80 m/s in altitudes from 0 to 2000 m.

For both configurations, increasing airspeed moves the Roll Mode towards higher absolute damping, i.e. towards a smaller Roll Time Constant. Further, both configurations show an unstable Spiral Mode for low airspeeds that moves towards (and with deployed landing gear even into) the left half plane for higher airspeeds. The characteristics of the Dutch Roll on the other hand significantly depend on the state of the landing gear. With retracted landing gear one can observe that the Dutch Roll is sufficiently stable over the whole envelope although its damping decreases with rising airspeed. With deployed landing gear on the other hand, the natural frequency of the Dutch Roll is significantly reduced for increasing airspeeds while the poles move towards (and for very high airspeeds into) the right half plane.

In addition to an assessment of the eigenvalues, the corresponding eigenvectors provide insight to the coupling of the axes. With a leading edge sweep of 55° the SAGITTA Demonstrator e.g. shows a strong roll-yaw-coupling which is easily observable from the high Φ/β ratio in the eigenvector of the Dutch Roll.

C. Stabilization Capability

We have seen in section III.B that for some points of the flight envelope the Dutch Roll poles come close to the imaginary axis or even cut across it. Hence, we will have a look at the general stabilization capability of the yaw controls, considering the nonlinearities and limitations of the actuation system before we actually design a controller based on the linear state space models.

For that purpose we will apply a modified version of the approach presented in [2], to determine the worst $\left(C_{n,\beta}^{G}\right)_S$, i.e. the most negative yawing moment sideslip derivative w.r.t. the center of gravity in stability axes, that still results in stabilization of the aircraft after a given disturbance in the angle of sideslip. The approach does not need the final controller design since it is assumed that the control surfaces run at their maximum rate to full deflection.

The difference between the actual stability derivative and the limit can be exhausted by tolerances and is hence an indicator for the criticality of yaw control of the UAV.

1) Yaw Controls Modeling

The yaw controls applied for the assessments in this section are characterized by 2nd order dynamics with rate saturation. Thereby the rate saturation is modeled as constant over the deflection range. The actual value depends on the aircraft's velocity and altitude as well as angle of attack.

At higher angles of sideslip, the yaw controls show an undesirable effect on $(C_n^G)_S$. For some angles of attack, yaw control deflections meant for stabilization of the aircraft, i.e. positive ζ_{equiv} at negative β and vice versa, initially result in a destabilizing $\Delta(C_n^G)_S$. This effect is worst in the vicinity of $\alpha = 2°$ and hence in the following the flaps are always evaluated for this angle of attack. The angle of sideslip shall be fixed to the initial disturbance applied for the respective assessment.

The yaw controls are assumed to be the only control input affecting $(C_n^G)_S$ and the commands for control deflection are provided to the actuators with a delay of $T_{Delay} = 20\,ms$ to simulate the processing and transmission of the signals.

2) Yaw Dynamics Modeling

The yaw dynamics of the configuration are approximated as a worst case without yaw damping by

$$\begin{bmatrix}\dot{r}_S\\ \dot{\beta}\end{bmatrix} = \begin{bmatrix}0 & N_\beta\\ -1 & 0\end{bmatrix}_S \begin{bmatrix}r_S\\ \beta\end{bmatrix} + \begin{bmatrix}\widehat{N}_{Ctrl}(\zeta_{equiv})\\ 0\end{bmatrix}_S \tag{2}$$

Following that worst case approach, we do not apply the dynamic yawing moment sideslip derivative

$$\left(C_{n,\beta}^{G}\right)_{Dyn} = \left(C_{n,\beta}^{G}\right)_B \cdot \cos\alpha - \frac{(I_{zz}^{G})_B}{(I_{xx}^{G})_B} \cdot \left(C_{l,\beta}^{G}\right)_B \cdot \sin\alpha \tag{3}$$

known as the Dynamic Directional Stability Parameter by Weissman [3] with trim angles of attack for the yawing dynamics since it would represent in case of the SAGITTA Demonstrator a less unstable configuration for all $\alpha \neq 0°$. Instead, N_β is calculated to be

$$N_\beta = \frac{\bar{q} \cdot S \cdot s}{(I_{zz}^{G})_S}\left(C_{n,\beta}^{G}\right)_S \tag{4}$$

with the yawing moment of inertia $(I_{zz}^{G})_S$.

For the assessment the absolute value of $\left(C_{n,\beta}^{G}\right)_S$ is increased successively in steps of $0.001\,1/rad$ until the disturbance can no longer be stabilized.

3) Disturbance to be Stabilized

The disturbance in the angle of sideslip to be stabilized is determined from an alleviated cross-wind gust as e.g. described in [4]. Subsequently nominal gusts of 30 ft/s and 15 ft/s equivalent airspeed are addressed.

The alleviated gust is obtained from scaling the nominal gust by the gust alleviation factor

$$K_{Alleviation} = \frac{0.88 \cdot \mu}{5.3 + \mu} \tag{5}$$

where μ is the flight mechanical mass, interpreted for a lateral gust as

$$\mu = \frac{2 \cdot \frac{m}{S}}{\rho \cdot s \cdot C_{Y,\beta}} \tag{6}$$

Thereby the sideforce sideslip derivative $C_{Y,\beta}$ is evaluated for zero angle of attack and zero angle of sideslip which is a good representation of the average $C_{Y,\beta}$ over the assessed envelope.

For a specified alleviated true airspeed cross-wind v and an absolute velocity V_{abs} prior to the disturbance, the initial angle of sideslip to be stabilized is determined to be

$$\beta_{Dist} = \arcsin\frac{v}{V_{abs}} \tag{7}$$

4) Criterion for Stabilization Capability

The so-called Cliff Edge Approach balances the destabilizing moment build-up due to a sideslip disturbance (indicated by the blue dotted line in Fig. 4) unregulated, i.e. without respecting controller action, against the counteracting control moment build-up (pictured by the green respectively red solid line in Fig. 4), which is a worst case approximation of the real effective moment build-up of a controlled aircraft.

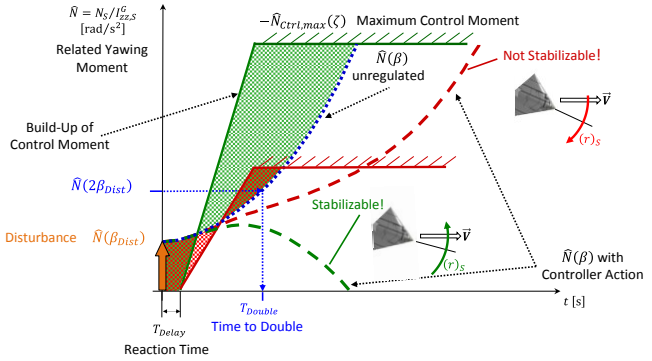

Fig. 4. Principle of the stabilization capability.

As criterion for the stabilization capability, we apply the conservative assumption that the aircraft can only be stabilized if the rotation rate resulting from the unregulated moment and the control moment can be brought back to zero. However, because of the conservatism a violation of the criterion not necessarily indicates the inability to stabilize the aircraft.

Graphically, the stabilization criterion is satisfied if the area between the unregulated moment and the control moment before the equilibrium is less or equal to the respective area after the equilibrium. In case the area after the equilibrium is larger than the area in advance (see e.g. the green example in Fig. 4), the control system is able to bring the disturbed angle back to its initial condition.

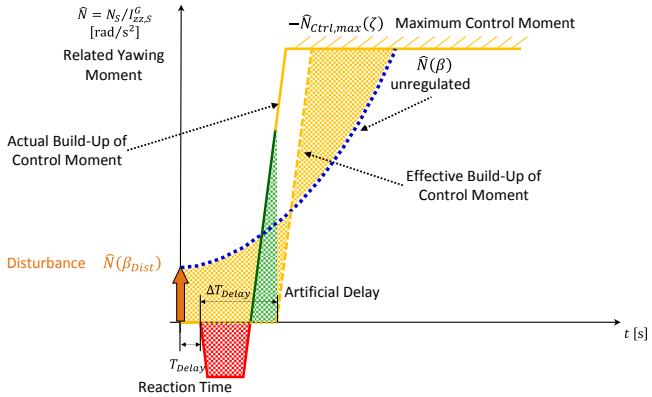

Fig. 5. Adjusted principle of the stabilization capability.

For the given yaw control characteristics that result in a destabilization of the aircraft during the first phase of control surface deflection, the approach described above needs to be adjusted. Without modifying the build-up of the unregulated yawing moment, the additional destabilization shall be represented by applying only the stabilizing contribution of the control moment with an artificial delay ΔT_{Delay}. In detail, it has been chosen to delay the effective build-up of control moment to the time when the rotation rate resulting from the actual control moment crosses zero, i.e. the negative area delimited by the actual related control moment (red in Fig. 5) and the respective positive area (green in Fig. 5) are equal.

5) Acceptable Stability Tolerances

Assessing the stabilization capability as described before over the different velocities and altitudes with retracted landing gear, we end up with a (conservative) limit for the worst stabilizable $\left(C^G_{n,\beta}\right)_S$ of

- $-0.011\ 1/rad$ with nominal gusts of $30\ ft/s$
- $-0.021\ 1/rad$ with nominal gusts of $15\ ft/s$

with only little changes over velocity and altitude.

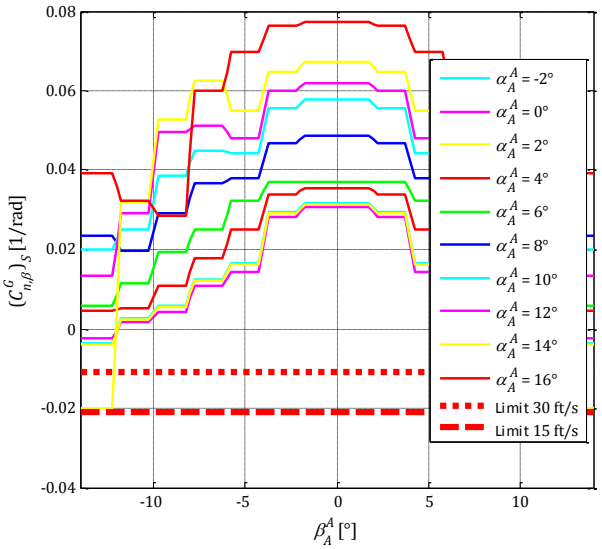

Fig. 6. Yawing moment sideslip derivative with stabilization limits.

Comparison of the two limits from above with the actual $\left(C^G_{n,\beta}\right)_S$ of the aircraft (with zero equivalent control deflections) in Fig. 6 gives an impression on the acceptable stability tolerances. With increasing absolute values of the angle of sideslip, the actual yawing moment sideslip derivative of Setup Wing approaches or even violates the limits depending on the considered α. In general, angles of attack in the vicinity of $\alpha = 0°$ leave only little margins for tolerances. Combinations of high angles of sideslip and attack are also critical (see especially $\alpha = 14°$ in Fig. 6) but typically outside of the operational envelope.

Highest uncertainties of the aircraft's stability can be tolerated in the vicinity of $\beta = 0°$, i.e. for small disturbances of the angle of sideslip, and (except for $\alpha = 14°$ in regions of high $|\beta|$) high angles of attack.

D. Envelope for Controller Design

Since the dynamics of the SAGITTA Demonstrator significantly vary over the envelope, it is reasonable to check for legitimate limitations prior to controller design.

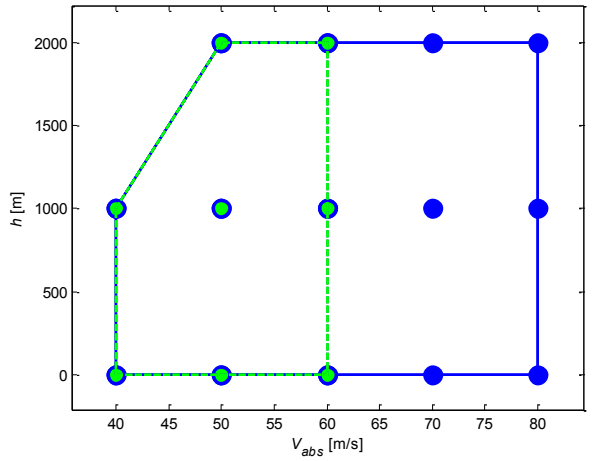

Fig. 7. Envelope assessed with Setup Wing for retracted landing gear (solid blue) and deployed landing gear (dashed green).

On the one hand, operational restrictions constitute limitations of the envelope. With deployed landing gear for example, an upper velocity limit of about 60 m/s results from the design loads of the landing gear system.

On the other hand, especially when designing a fixed-gain controller for a minimum functionality of the BFCS, it may be appropriate to exclude operational almost irrelevant regions from the envelope that would otherwise provide a design driver. The poles of the Spiral Mode of Setup Wing with retracted landing gear e.g. lie close together for velocities of and above 40 m/s and move significantly to the right for velocities below.

The envelope resulting for Setup Wing from respective considerations is shown in Fig. 7.

IV. Approach to Controller Structure and Gain Design

A. Get in Touch with the Dynamics

After the analysis of the inherent dynamics is performed and before starting the structural design of control laws, it is important to understand the effect of candidate measurements that can be used for feedback design on the plant's dynamics. A well-established method is the analysis of the Root Locus for each transfer function in scope. For SISO systems this method can be directly used for gain design. For MIMO systems the method provides qualitative insight, since simultaneous feedbacks of multiple variables affect each other.

The analysis leads to the choice of the following feedbacks as candidate measurements that will be used in further development steps of the controller for the lateral motion:

- Lateral Acceleration
- Yaw Rate
- Roll Rate
- Bank Angle

All of these measurements can be obtained from the AHRS.

B. MIMO Gain Design Methods

Several Multi-Input Multi-Output Gain Design Methods have been evaluated regarding their applicability to the problem of lateral control of the SAGITTA Demonstrator.

The focus was on the following:

- The possibility to explicitly place the poles for the rigid body system to a certain position or region in the complex plane: this design shall result in conventional closed-loop modes, which shall enable a simpler analysis of the closed-loop dynamics and a better understanding of the system's behavior.
- The resulting order of the controller.
- The ability to take influence on the controller structure.

We have studied the following approaches: LQR, H_∞, Multi-Model Eigenstructure Assignment, Model Reference Direct Eigenstructure Assignment, and Constrained Eigenstructure Assignment.

Due to the limited influence on the pole position using LQR and H_∞ these approaches were excluded from further analysis. The different Eigenstructure Assignment approaches are analyzed in subsequent sections.

C. Classical and Multimodel Eigenstructure Assignment

Eigenstructure Assignment is a powerful method for linear controller design. By using *m* feedback variables (either states for state feedback or outputs for output feedback) the designer is able to place *m* eigenvalues exactly to a predefined position in the complex plane. Furthermore the designer is given the freedom to modify *r* entries of the eigenvector arbitrary (*r* equals the number of independent control inputs to the plant to be controlled). The result of the design process is the feedback matrix $K \in \mathbb{R}^{rxm}$. We will briefly recall the general idea of Eigenstructure Assignment.

Let us consider the dynamic system

$$\begin{aligned} \dot{x} &= Ax + Bu \\ y &= Cx \end{aligned} \tag{8}$$

for the output feedback case, with the following control law: $u = -Ky$. This results in a closed-loop system defined by:

$$\begin{aligned} \dot{x} &= (A - BKC)x \\ y &= Cx \end{aligned} \tag{9}$$

For all desired closed-loop eigenvalues λ_i and the corresponding achievable eigenvectors v_{i_a} the following relation holds:

$$[\lambda_i I - A + BKC]v_{i_a} = 0 \tag{10}$$

By rewriting (10) to

$$M \begin{bmatrix} v_{i_a} \\ z_{i_a} \end{bmatrix} = 0 \tag{11}$$

with $M = [\lambda_i I - A \quad B]$ and $z_i = KCv_{i_a}$ it can be seen, that the vector $\begin{bmatrix} v_{i_a} \\ z_{i_a} \end{bmatrix}$ must lie in the Nullspace of the matrix M. Since the desired eigenvector v_{i_d} (specified by the designer according to dynamics requirements) is not necessarily

collinear to v_{i_a}, the desired eigenvector must be projected into the Nullspace of the matrix M generating the achievable vectors v_{i_a} and z_{i_a}. Subsequently the feedback matrix can be calculated according to (12).

$$K = Z(CV)^{-1} \tag{12}$$

with $Z = [z_{1_a} \dots z_{m_a}]$ and $V = [v_{1_a} \dots v_{m_a}]$.

One of the main challenges of the Controllability Study is to find a single gain set that is able to stabilize the aircraft over the entire envelope. The chosen approach for the problem at hand is Multi-Model Eigenstructure Assignment (MEA) [5]. The MEA approach allows the application of different state space models for the different dynamic modes under consideration in the gain design procedure. The particular state space model may represent the worst case behavior for the distinct mode at the chosen operation point in the envelope. This method is usually applied to generate robust controllers for plants that are subject to uncertainties. In our case the approach is used to generate a fixed-gain (not scheduled over dynamic pressure) controller that is suitable for stabilization of the aircraft throughout the whole flight envelope. The variations throughout the envelope are considered as uncertainties.

In order to apply the MEA approach we first need to identify the critical points of the envelope with respect to their stability properties.

After the critical points of the envelope have been identified, the classical Eigenstructure Assignment is provided with a dedicated state space model for each mode and results in a robust closed-loop design. For algorithm details the reader is referred to [6].

D. Drawbacks of the Eigenstructure Assignment and Approaches to Overcome the Problems

Classical Eigenstructure Assignment and its pitfalls are well known. Two of them will be presented here.

On the achievability of the desired eigenvector: The inputs to Eigenstructure Assignment are the specification of m desired eigenvalues and corresponding desired eigenvectors (Note: only relevant entries for the achievement of closed-loop requirements, e.g. Φ and β for decoupling of yaw- and roll motion, need to be specified). Usually the specified entries of the eigenvector are not perfectly achievable. To overcome this problem the Nullspace N of the Matrix M is calculated to project the desired eigenvector into the achievable space.

We observe that the magnitude of the resulting entries in K calculated by Eigenstructure Assignment are highly dependent on the selection of the desired eigenvector. A bad selection of the desired eigenvector may lead to large entries in the feedback matrix and thus result in non-robust high gain controllers.

To get a deeper understanding of the dynamic characteristics [7] suggests to analyze the singular value decomposition of the column space of

$$L_i = (\lambda_i I - A)^{-1} B \tag{13}$$

Originating from equation (14),

$$(A - BKC)v_{i_a} = \lambda_i v_{i_a} \tag{14}$$

which is the definition for the system's closed-loop eigenvalues and eigenvectors, we get

$$(\lambda_i I - A)v_{i_a} = -BKC v_{i_a} \tag{15}$$

and finally

$$v_{i_a} = L_i(-KC)v_{i_a} \tag{16}$$

From (16) it is obvious that the matrix multiplication of the output matrix C and the feedback matrix K must compensate the rotation and scaling by L_i. Thus, by analysis of the left-singular vector of L_i and the corresponding singular values the designer gets the direction of high amplification and thereby hints for the selection of the desired eigenvectors that eventually lead to feedback gains of small magnitude.

Since the eigenvectors leading to small entries in K are not always compliant with the required dynamic properties of the closed-loop system, the designer must trade low-gain amplification and performance. For a possible implementation of such a trade-off, the reader is referred to [8].

On the limitations of resulting feedback structure: The result of gain design using Eigenstructure Assignment is a feedback matrix $K \in \mathbb{R}^{rxm}$ where each output is fed back to each input. This limits the designer's choice of the controller structure and makes the controller more complex. Andry et al. introduced in [9] the so-called Constrained Eigenstructure Assignment, which allows the suppression of certain feedbacks to certain inputs.

In preparation of the Constrained Eigenstructure Assignment, the open-loop system is transformed with the transformation matrix T as follows:

$$\begin{aligned} \tilde{A} &= T^{-1}AT \\ \tilde{B} &= T^{-1}B \\ \tilde{C} &= CT \end{aligned} \tag{17}$$

with $T = [\, B \mid P \,]$ and P being any matrix such that the $rank(T) = n$ (number of states of the system).

The corresponding transformation of the system's state and eigenvector is done according to (18).

$$\begin{aligned} \tilde{x} &= T^{-1}x \\ \tilde{v}_i &= T^{-1}v_i \end{aligned} \tag{18}$$

By using the proposed transformation, the new input matrix appears in the following form:

$$\tilde{B} = \begin{bmatrix} I_r \\ 0 \end{bmatrix} \tag{19}$$

From now on, for reasons of convenience we drop the $\tilde{\square}$ notation and consider the transformed system.

By partitioning (15) as follows

$$\begin{bmatrix} \lambda_i I_r - A_{11} & -A_{12} \\ -A_{21} & \lambda_i I_{n-r} - A_{22} \end{bmatrix} \begin{bmatrix} f_i \\ w_i \end{bmatrix} = \begin{bmatrix} I_r \\ 0 \end{bmatrix} (-KC) \begin{bmatrix} f_i \\ w_i \end{bmatrix} \quad (20)$$

we can derive equation (21)

$$(\lambda_i I_r - A_{11})\, f_i - A_{12} w_i = (-KC) \begin{bmatrix} f_i \\ w_i \end{bmatrix} \quad (21)$$

and rewrite the equation in a compact form to

$$\lambda_i f_i - A^{\star} v_i = (-KC) v_i \quad (22)$$

with $A^{\star} = [A_{11}\ A_{12}]$ and $v_i = \begin{bmatrix} f_i \\ w_i \end{bmatrix}$, leading to the solution for the feedback matrix

$$K = -\Psi\, (CV)^{-1} \quad (23)$$

with $\Psi = (F - A^{\star} V)$, where $F = [\lambda_1 f_1 \dots \lambda_n f_n]$.
For each row k_i of the matrix K and respective each row ψ_i of Ψ the following equation holds:

$$k_i = -\psi_i\, (CV)^{-1} \quad (24)$$

For suppression of the entry k_{ij} in vector k_i we just need to remove the j^{th} row from the expression CV and calculate the results for k_i using e.g. the pseudoinverse.

Another interesting approach to Eigenstructure Assignment that enables the suppression of certain feedback entries and does not require an explicit definition of the desired eigenvectors is the so-called Model Reference Direct Eigenstructure Assignment that is applied to the lateral dynamics of a General Aviation aircraft in [10]. The approach is based on the construction of a closed-loop system matrix using a controller with parametric gains. After the closed-loop system is constructed, the designer uses his knowledge about the system to shape its eigenstructure. In the first step, he cancels the entries in the state space model that describe the coupling terms of yaw- and roll motion. In subsequent steps he treats the dynamic modes as decoupled and calculates the gains based on comparison of coefficients of the respective low order transfer functions. The approach shown in [10] is intuitive and physically motivated and thus provides a good method for systems where decoupling of yaw- and roll motion is desirable and – even more important – physically achievable.

For the gain design of the controller of the Controllability Study, the best of the proposed Eigenstructure Assignment approaches has been combined to a very flexible and robust approach. The calculation procedure combines MEA with Constrained Eigenstructure Assignment and is straightforward:

1) Define desired closed-loop eigenvalues and eigenvectors.
2) Choose state space models representing critical dynamic modes.
3) Perform the projection of desired eigenvectors to Nullspace to generate achievable eigenvectors.
4) Transform the state space models and the achievable eigenvectors provided to the EA as described by the CEA method.
5) Select entries of K to be suppressed and perform the calculation of K according to (23).

E. Discussion on Controller Structure

The controller structure design was mainly driven by the requirements stated in II.B and the design guideline to select a physically motivated clear structure where each feedback shall have an obvious function regarding the modification of the dynamics of the aircraft's lateral motion. After having identified the useful feedbacks as described in IV.A the design depicted in Fig. 8 was derived.

The resulting structure can be divided into a decoupling control allocation, a rate loop, and an attitude loop.

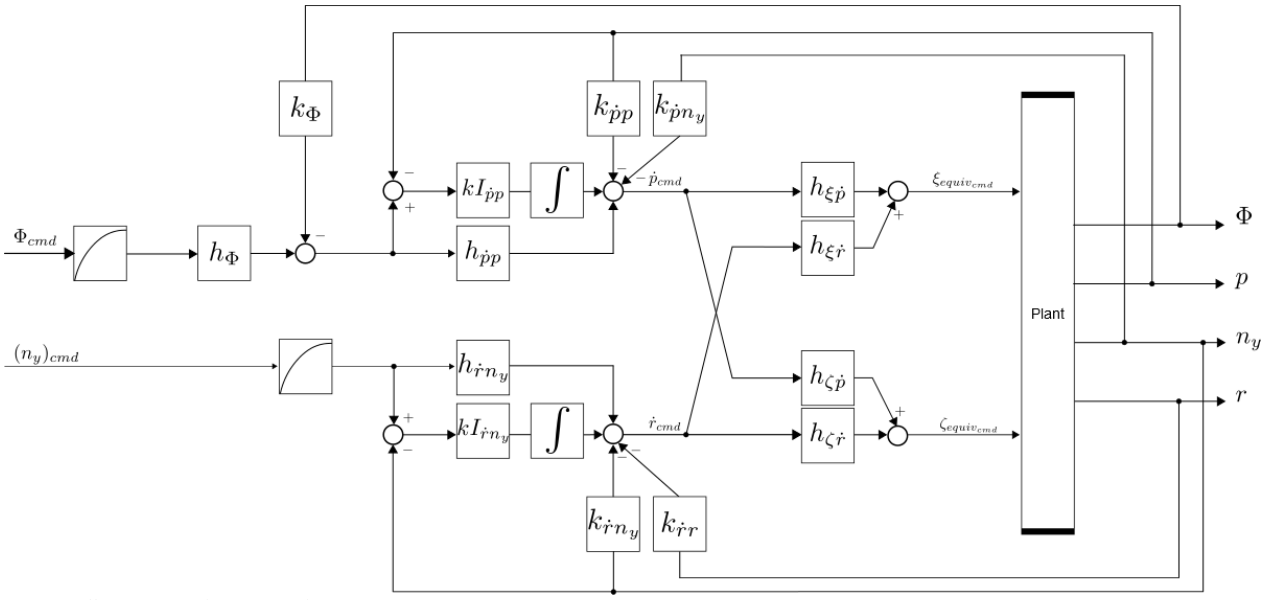

Fig. 8. Controller structure for Setup Wing.

Control Allocation: The Control Allocation (CA) consists of the gains $h_{\xi\dot{p}}$, $h_{\xi\dot{r}}$, $h_{\zeta\dot{p}}$, and $h_{\zeta\dot{r}}$ and is set up according to [10]. The gains provide a decoupling regarding the control-roll-moment L_c and control-yaw-moment N_c or corresponding roll- and yaw acceleration commands respectively.

Rate Loop: The Rate Loop consists of a proportional and integral roll rate feedback to $\dot{p}_{cmd}$ and a yaw rate feedback to $\dot{r}_{cmd}$. While the roll rate feedback moves the Roll Mode's pole towards small Roll Time Constant, the yaw rate feedback is responsible for the modification of the Dutch Roll poles towards higher frequencies and thus towards higher absolute damping. The latter feedback is essential for stabilization of the aircraft's unstable Dutch Roll at higher velocities.

Attitude Controller: On top of the rate feedbacks, an attitude controller is implemented. The bank angle feedback to $\dot{p}_{cmd}$ stabilizes the unstable Spiral Motion for lower speeds, while the feedback of lateral acceleration n_y is used to substitute the unavailable feedback of the angle of sideslip β. By using the feedback of n_y to $\dot{r}_{cmd}$ the frequency of the Dutch Roll can be increased and thus a higher absolute damping is achieved.

Cross-feedback from n_y to $\dot{p}_{cmd}$ is essential for reduction of roll-yaw couplings which are extraordinary high for the SAGITTA Demonstrator.

Because of the diamond shape of the aircraft and the absence of vertical tail in the Setup Wing, its visibility is poor and visual determination of its attitude is very difficult. To give the External Pilot the option to estimate the aircraft's attitude based on the current stick deflections at the radio transmitter when the aircraft can hardly be seen, it was decided to implement a bank angle command system. Virtual flight tests that have been performed during the Manual Landing Study confirmed the suitability and even necessity of an attitude control system for such an aircraft.

In order to enable a landing with cross-wind a lateral acceleration command system was implemented which provides the possibility to control the angle of sideslip and thus the functionality to perform a de-crab maneuver.

V. Open- and Closed-Loop Analysis of the System

A. Frequency Domain Analysis

1) Pole-Zero Map

In Fig. 9 the Pole-Zero Maps of the closed-loop system are depicted. In particular, we see in 1) the actuators, 2) the Dutch Roll, 3) the Roll Motion, 4) Spiral Mode and controller integrators.

The chosen controller manages to move the poles to the left half plane. However, since gain scheduling has not been an option during the Controllability Study, the closed-loop poles are not concentrated in close vicinity to the desired pole positions used for the controller design but significantly vary over the flight envelope. In order to achieve overall stability and acceptable dynamics with the fixed-gain controller, this issue of poles deviating from the desired poles has been addressed by applying rather critical points of the flight envelope for gain design and by choosing desired poles with e.g. higher damping in order to give some margin to those envelope points that have worse plant dynamics than the design points. Using by default the worst points of the envelope for gain design is not recommendable since these points do not necessarily represent typical operating points of the aircraft. A respective design would not be balanced since the dynamics and performance during most parts of the mission would be completely out of scope.

2) Nichols Plot

When manually tuning single gains of a controller (which is recommended by the authors only for getting in touch with the plant's characteristics and to get an impression of the overall achievable dynamics), it is easily possible to assess the effect of the considered gain on the closed-loop system's stability robustness by determining phase and gain margin from the corresponding open-loop dynamics, i.e. the dynamics when cutting the loop open at the gain, in a Bode plot. Thereby the distance to the critical point

$$\phi_0 = 180° \pm 360° \; @ \; A_0 = 0 \; dB$$

is considered only one dimensional. The phase margin is determined at a gain of $0\,dB$, whilst the gain margin is determined at a phase of $180° \pm 360°$. Everything in between these points is not considered.

A more detailed picture on the stability robustness of the closed-loop system can be gained from assessment of the open-loop dynamics in the Nichols chart. Introducing the so called Nichols Diamond, i.e. an area around the critical point in the phase-gain-plane of the Nichols chart that indicates a certain level of robustness when avoided, we can easily check the robustness by comparison with a given Nichols Diamond or by determining the biggest diamond that is not violated.

During the Controllability Study, two different Nichols Diamonds with the following specification have been applied:

- The corners of the outer diamond are specified by
  $\phi_0 = 145^\circ \pm 360^\circ \; @A_0 = \pm 3\,dB$
  $\phi_0 = 180^\circ \pm 360^\circ \; @A_0 = \pm 6\,dB$
  $\phi_0 = 215^\circ \pm 360^\circ \; @A_0 = \pm 3\,dB$
- The corners of the inner diamond are specified by
  $\phi_0 = 145^\circ \pm 360^\circ \; @A_0 = \pm 1.5\,dB$
  $\phi_0 = 180^\circ \pm 360^\circ \; @A_0 = \pm 4.5\,dB$
  $\phi_0 = 215^\circ \pm 360^\circ \; @A_0 = \pm 1.5\,dB$

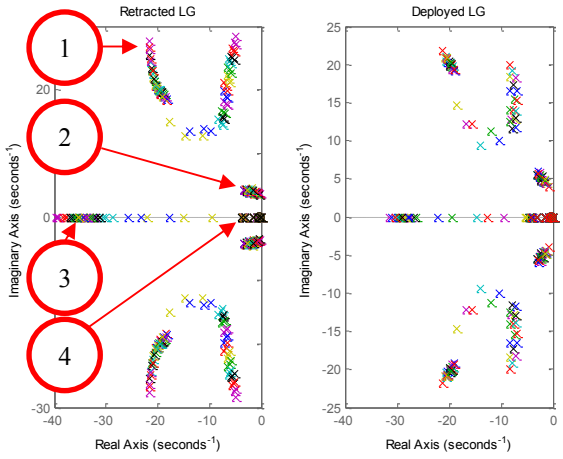

Fig. 9. Pole-zero map of the closed-loop system for retracted and deployed landing gear.

Whilst the outer diamond specifies the clearance boundaries for the nominal plant, the inner diamond is typically used for evaluation of the plant with the worst combination of uncertainties.

After controller design, there is only little benefit in assessing the dynamics cut open at the individual controller gains. Instead, it is reasonable to cut the closed-loop open at the controls in front of / behind the control allocation (a.k.a. bottleneck cut) and at the sensors.

By means of the cut at the controls behind the CA, we gain information on the robustness towards uncertainties in the control effectiveness and dynamics of the control surfaces.

By means of the cut at the sensors, we gain information on the robustness towards uncertainties in the sensor dynamics.

By means of the cut in front of the CA, we gain insight into the overall amplification of the particular angular moment channel.

Fig. 10 exemplarily shows a Nichols chart of the lateral dynamics cut open at $\dot{p}_{cmd}$ with an additional time delay of $20\,ms$. Thereby the additional time delay, is applied to all outputs of the controller (including the output that is cut open for the open-loop). For better readability, the stability margins are additionally shown over the velocity. The color coding of the plots of the stability margins indicates the relative magnitude of the values (red indicates large values, blue indicates small values). The filled areas indicate the variation of the margins over the fuel mass. The color of the filled area is determined by the smallest value along its edges.

We can see, that the controller design does not satisfy the robustness requirements (i.e. the frequency response is penetrating the diamond shape areas depicted in Fig. 10). Since the Nichols Diamond is penetrated from below, we can conclude, that the amplification in the $\dot{p}$ channel is too high. This is the result of the designer's attempt to achieve good decoupling of the roll- and yaw motion and to suppress the build-up of high bank angles during lateral gusts (which will be discussed later in the paper). From this analysis we can conclude, that further iterations of controller design must trade performance of the controller against more robustness.

3) *Roll-Yaw Coupling*

As already mentioned in III.B extremely high roll-yaw couplings of the SAGITTA Demonstrator must be reduced in order to achieve acceptable flying qualities. The roll-yaw coupling can be quantified by comparison of the entries of Φ and β in the Dutch Roll eigenvector. The comparison of the uncontrolled and closed-loop system's Φ/β is depicted in Fig. 11. Especially for moderate speeds the controller shows significant reduction of the roll-yaw coupling.

B. *Time Domain Analysis*

During the Controllability Study we have analyzed the tracking performance and the aircraft's response to lateral

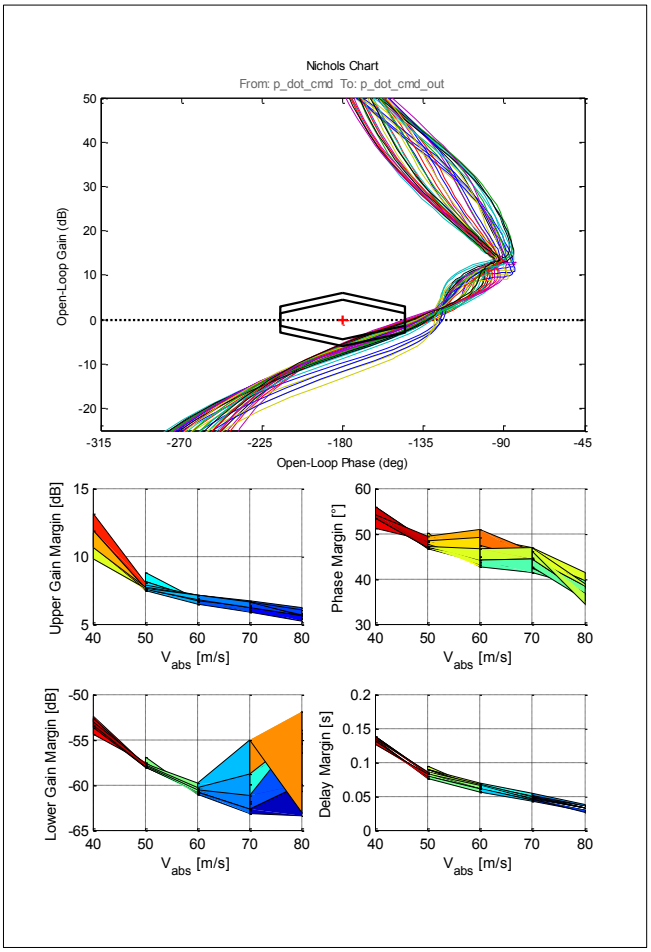

Fig. 10. Nichols chart of the lateral motion, cut at $\dot{p}_{cmd}$.

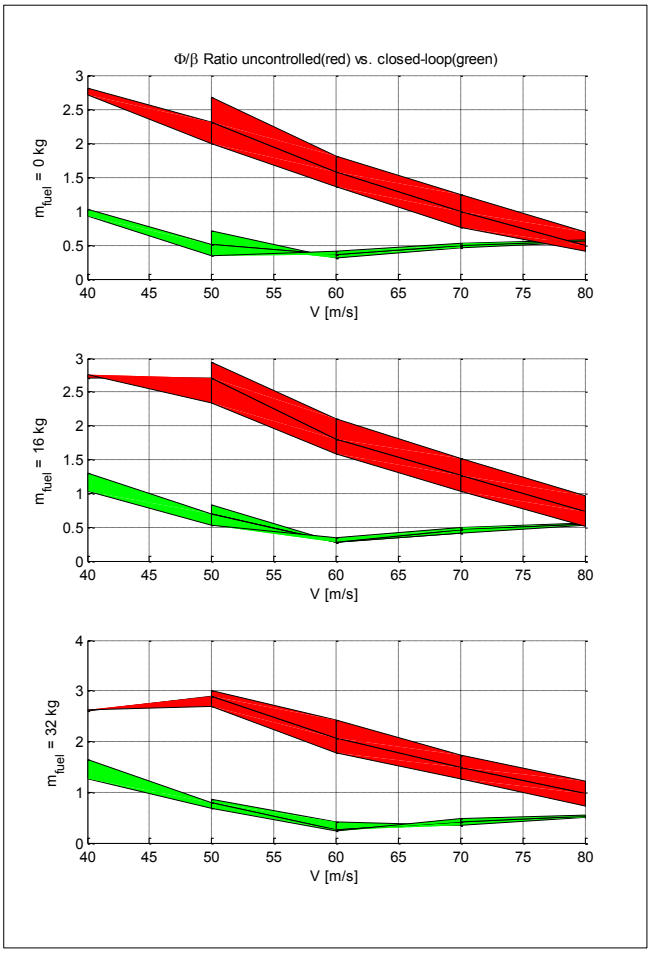

Fig. 11. Roll-Yaw Coupling: uncontrolled vs. closed-loop plant.

gusts. In this paper we will focus on the gust analysis and omit the tracking performance.

The analysis of the aircraft's closed-loop reaction to lateral gusts is based on the Discrete Gust Design Criteria in [11]. The following gust shape is assumed:

$$v = \frac{U_{ds}}{s}\left[1 - \cos\left(\frac{\pi s}{H}\right)\right] \tag{25}$$

where U_{ds} is the design gust velocity in equivalent airspeed, s is the distance penetrated into the gust, H is the gust gradient which is the distance (in feet) perpendicular to the aircraft flight path for the gust to reach its peak velocity. Thereby the design gust velocity is calculated as

$$U_{ds} = U_{ref} F_g \left(\frac{H}{350}\right)^{\frac{1}{6}} \tag{26}$$

where U_{ref} is the reference gust velocity in equivalent airspeed (set to $U_{ref} = 30\,ft/s$) and F_g is the Flight Alleviation Factor (here set to $F_g = 1$, which is the worst case scenario). The aircraft's closed-loop response was investigated for $H = [30, 190, 350]\,ft$.

In Fig. 12 the time series for a lateral gust of the length $H = 190\,ft$ is shown. We see the progression of kinematic angle of sideslip β_K and aerodynamic angle of sideslip β_A and the gust input β_W that can be calculated according to (7). The different magnitude and length of the gust inputs result from the application of the gust at different velocities. For all points displayed in the plot we see a buildup of moderate aerodynamic sideslip angles (up to 6°) and a fast attenuation of β_A to zero. The actuation activity shown in Fig. 13 is well within limits (Note: The actuators are capable to provide a maximum rate of $100\,°/sec$ and a maximum deflection of 45°), whilst the analysis at $H = 30\,ft$ resulted in exceedance of the maximum allowed rates and deflections. Therefore, the linear simulation brought no valid results for the particular case $H = 30\,ft$.

VI. Summary

In this paper insight was given into the work on the Controllability Study that was performed in preparation of the Preliminary Design Review of the SAGITTA Demonstrator.

The analysis of the stabilization capability provided initial information on the suitability of the novel split-flap design for stabilization of the yaw motion. The destabilizing effect for small control surface deflections was considered by introduction of an equivalent additional time delay in the actuator. This resulted in the specifiaction of tolerable uncertainties for the particular stability relevant coeffient.

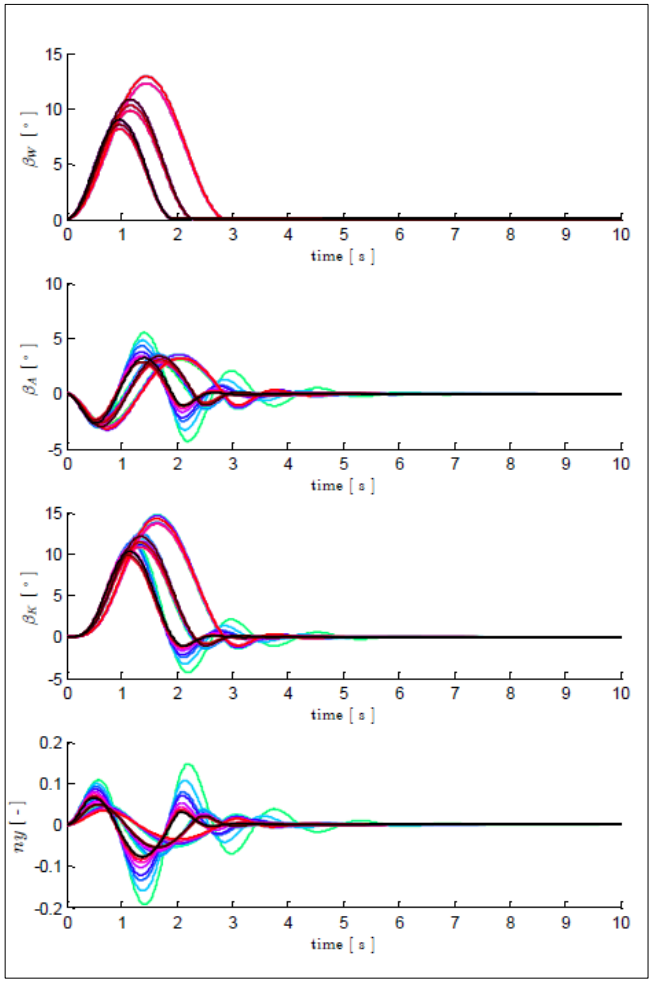

Fig. 12. Disturbance reaction to lateral gusts (H = 190 ft).

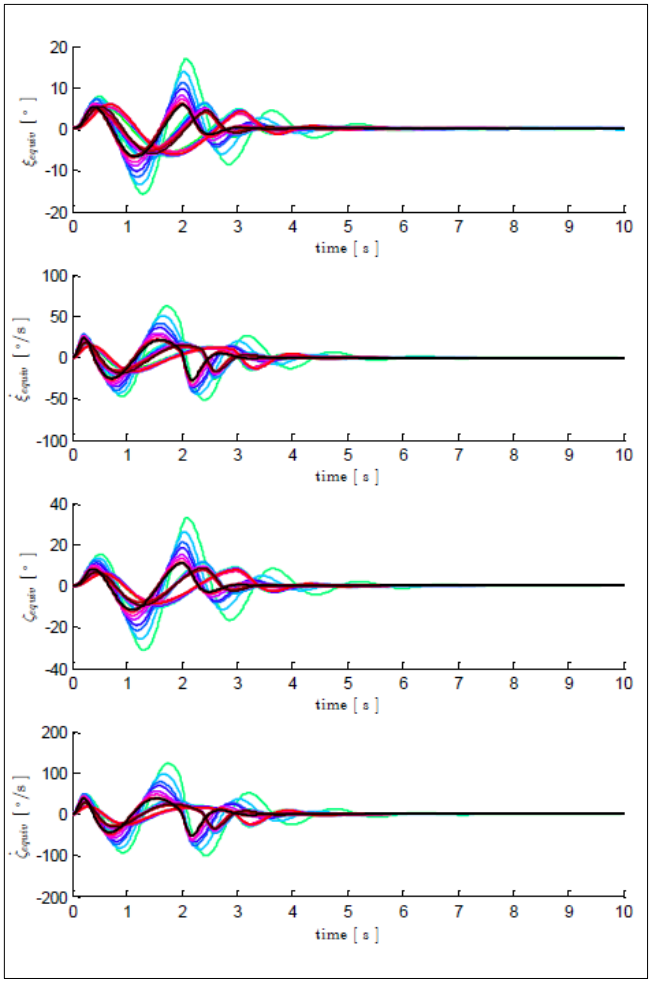

Fig. 13. Actuators disturbance reaction to lateral gusts (H = 190 ft).

Further, a suitable preliminary controller structure was developed and an appropriate approach to gain design for the lateral motion that is compliant with the requirements stated in II.B was derived. The combination of Constrained Eigenstructure Assignment and Multi-Model Eigenstructure Assignment resulted in a relatively simple fixed-gain controller leading to classical, easy to analyze closed-loop eigenmodes (i.e. Dutch Roll, Roll Motion and Spiral Motion) over the entire envelope.

The open- and closed-loop behavior of the system were investigated by means of frequency- and time-domain analysis.

Nichols charts were provided with cuts in front and behind the Control Allocation and at the sensor's output for analysis of robustness of the closed-loop system. From the assessment of Nichols charts we derived requirements on tolerable time-delays in the system and hints on the trade-off between performance and robustness. The gust analysis led to a forecast regarding tolerable atmospheric disturbances.

Having elaborated details on the expected closed-loop stability and performance properties of the SAGITTA Demonstrator the Preliminary Design Review was succesfully passed.

VII. References

[1] NASA, Systems Engineering Handbook, Washington, D.C.: NASA, 2007.

[2] M. Geiser and M. Heller, "Flight Dynamics Analysis and Basic Stabilization Study in Early Design Stages of the SAGITTA Demonstrator UAV," in *DLRK*, Berlin, 2012.

[3] R. Weissman, "Status of Design Criteria for Predicting Departure Characteristics and Spin Susceptibility," *Journal of Aircraft,* vol. 12, no. 12, pp. 989-993, 1975.

[4] EASA, Certification Specification for Normal, Utility, Aerobatic, and Commuter Category Aeroplanes CS-23, Amendment 3, EASA, 2012.

[5] C. Döll, J. Magni and Y. Le Gorrec, "A Modal Multi Model Approach," in *Lecture Notes in Control and Information Sciences Volume 224*, Berlin, Heidelberg, New York, Springer, 1997, pp. 258-277.

[6] M. Heller, F. Holzapfel and S. Gottfried, "Robust Lateral Control of Hypersonic Vehicle," in *AIAA Guidance, Navigation and Control Conference and Exhibit*, Denver, 2000.

[7] J. Griffith, "Comments on Achievable Eigenvectors," in *American Control Conference*, Idaho, 1986.

[8] J. B. Davidson, "Gain Weighted Eigenspace Assignment," NASA Langley, Hampton, 1994.

[9] A. Andry, E. Shapiro and J. Chung, "Eigenstructure Assignment for Linear Systems," *IEEE Transactions on Aerospace and Electronic Systems,* Vols. AES-19, no. 5, 1983.

[10] M. Heller, "Lateral Fly by Wire Control System Dedicated to Future Small Aircraft," in *CEAS Euro GNC*, Delft, 2013.

[11] EASA, Certification Specification for Large Aeroplanes CS-25, Amendment 3, EASA, 2007.